

Effects of SiO₂ substitution on wettability of laser deposited Ca-P biocoating on Ti-6Al-4V

Yuling Yang · Sameer R. Paital ·
Narendra B. Dahotre

Received: 10 February 2010 / Accepted: 20 May 2010 / Published online: 15 June 2010
© Springer Science+Business Media, LLC 2010

Abstract Silicon (Si) substitution in the crystal structure of calcium phosphate (CaP) ceramics has proved to generate materials with improved bioactivity than their stoichiometric counterpart. In light of this, in the current work, 100 wt% hydroxyapatite (HA) precursor and 25 wt% SiO₂-HA precursors were used to prepare bioactive coatings on Ti-6Al-4V substrates by a laser cladding technique. The effects of SiO₂ on phase constituents, crystallite size, surface roughness, and surface energy of the CaP coatings were studied. Furthermore, on the basis of these results, the effects and roles of SiO₂ substitution in HA were systematically discussed. X-ray diffraction analysis of the coated samples indicated the presence of various phases such as CaTiO₃, Ca₂SiO₄, Ca₃(PO₄)₂, TiO₂ (Anatase), and TiO₂ (Rutile). The addition of SiO₂ in the HA precursor resulted in the refinement of grain size. Confocal laser microscopy characterization of the surface morphology demonstrated an improved surface roughness for samples with 25 wt% SiO₂-HA precursor compared to the samples with 100 wt% HA precursor processed at 125 cm/min laser speed. The addition of SiO₂ in the HA precursor resulted in the highest surface energy, increased hydrophilicity, and improved biomineralization as compared to the control (untreated

Ti-6Al-4V) and the sample with 100 wt% HA as precursor. The microstructural evolution observed using a scanning electron microscopy indicated that the addition of SiO₂ in the HA precursor resulted in the presence of reduced cracking across the cross-section of the bioceramic coating.

1 Introduction

A significant amount of work has been performed on synthetic biomaterials due to their high demands for replacing damaged and degraded organs and tissues [1]. Among these various potential biomaterials, load bearing implant materials to heal skeletal defects caused due to trauma, old age, and injury are on the continuous rise. As a potential scaffold biomaterial, these materials are expected to provide mechanical support for bone tissue growth, enhancement in cell proliferation, and a tissue-specific differentiation at the interface [2–4]. In light of this, several researchers have synthesized CaP based bioactive hydroxyapatite (Ca₁₀(PO₄)₆(OH)₂, HA) coatings on Ti-6Al-4V substrates and studied their in vitro bioactivity and in vitro biocompatibility [5, 6]. These HA based bioceramics mimic the naturally occurring bone mineral in terms of their chemical composition and crystallographic structure and hence, allow for direct bone bonding by attachment, proliferation, and differentiation of bone forming cells. However, some of the recent studies on HA coatings have limited their scope for implant applications, owing to the adverse reactions found in vitro and in vivo [7], low bonding strength between the HA and substrate, and poor mechanical properties of the coating. Hence, to overcome these limitations there has been a considerable interest in developing new bioactive ceramic coatings based on bio-glass compositions such as Na₂O–CaO–SiO₂–P₂O₅ [8],

Y. Yang
Department of Physics, Northeastern University,
Shenyang 110004, China

Y. Yang · S. R. Paital · N. B. Dahotre (✉)
Department of Materials Science and Engineering,
The University of Tennessee, Knoxville, TN 37996, USA
e-mail: ndahotre@utk.edu; Narendra.Dahotre@unt.edu

Present Address:
N. B. Dahotre
Department of Materials Science and Engineering,
University of North Texas, Denton, TX 76203, USA

wollastonite (CaSiO_3) [9], and dicalcium silicate (Ca_2SiO_4) [10].

In most of the above compositions, the presence of SiO_2 is found to be in common, since SiO_2 can easily form a Si-OH functional layer under in vivo and in vitro conditions and there by enhance the mineralization of an apatite like phase at the interface between the bioceramic coating and hard tissue. The role of Si as an essential element for higher biological organisms was discovered in the 1970s through the studies by Carlisle [11], Schwarz [12], and Seaborne [13]. It was reported that Si is present at a level of ~ 1 ppm in the serum, 2–10 ppm in the liver, kidney, lung, and muscle, 100 ppm in the bone and ligaments, and 200–600 ppm in cartilage and other connective tissues [14]. Hence, Si in particular has been found to be essential for normal bone and cartilage growth and development [15]. Another reason for SiO_2 being used as the basement of above systems is that it can act directly in the mineralization process, where aqueous Si, in the form of orthosilicic acid ($\text{Si}(\text{OH})_4$), is able to induce the precipitation of HA from electrolyte solutions in the presence of proteins that normally inhibit its precipitation [16, 17]. Due to the above beneficial properties of SiO_2 in biomaterials, SiO_2 (or Si) substitution in the CaP bioceramics has been an area of active research. The synthesis and characterization of SiO_2 or Si fortified HA and α -tricalcium phosphates have been the focus of many research efforts [15, 18–25]. In all of these works, the synthesis method, the phase composition, the effect of Si on biological activity, and the role of Si on the grain growth, were extensively studied. It was concluded that the phase composition of the materials highly depend on the Ca/(P + Si) and Ca/P ratios of the system, the level of Si addition, and the method of introducing Si to CaP [15]. Furthermore, Si tends to inhibit the grain growth to generate materials with fine structures [19, 23, 24]. The work by Patel et al. compared the biological activity of Si-HA and HA granules and reported a 14.5% increase in bone in-growth in Si-HA versus HA controls [25].

Most of the above studies on the composite coatings (SiO_2 -HA or Si-HA) focus on the synthesis methodologies, the biological activity, the influence of SiO_2 or (Si) addition on the grain growth, and the biological response to an implant. There are not many efforts towards understanding effects of SiO_2 (or Si) addition on the wettability and surface energy of these composite (SiO_2 -HA or Si-HA) ceramic coatings except the work by Thian et al. [26]. In their work, the authors [26] used an electrospraying technique to synthesize nano HA, carbonate substituted nano HA and silicon substituted nano HA on glass substrates. The authors demonstrated that the modification of nano-apatite by silicon resulted in improved hydrophilicity and thereby enhanced osteoblast cell attachment, proliferation

and protein expression as compared to the nano HA coating and carbonate substituted nano HA coating. Hence, it is very important to critically study and understand the role of SiO_2 or (Si) addition on the wetting behavior of these composite ceramic coatings. Also, as implant materials when placed inside a human body initially come in contact with the body fluid, it further controls the adsorption of proteins followed by attachment of cells to the implant surface. Hence, an understanding of the above can aid in designing an appropriate precursor (SiO_2 or Si-HA composite) to enhance its wettability and thereby tune its bioactivity and biocompatibility efficiently.

Therefore, in the present effort the effect of SiO_2 addition on the wettability and bioactivity of laser deposited CaP coating on Ti-6Al-4V substrate has been discussed. Here, a highly intense laser beam was used to melt the precursor (HA and SiO_2 -HA) and the Ti-6Al-4V substrate to get a micro-textured multi-phase coating and a metallurgical bonding at the interface. The effects of SiO_2 on the phase constituents, the crystallite size, the surface roughness, and the surface energy of the micro-textured CaP coating are studied. Furthermore, on the basis of these results, the effects and roles of SiO_2 addition in HA are systematically discussed.

2 Materials and methods

2.1 Sample preparation and laser processing

Ti-6Al-4V substrate coupons of dimensions 100 mm \times 50 mm \times 3 mm were cut from the rolled sheets using an abrasive cutter. Before being coated with the precursor, all substrate coupons were polished using a 30 μm grit SiC emery paper and then rinsed with acetone to get a clean surface free from rust and oxides. Hydroxyapatite ($\text{Ca}_{10}(\text{PO}_4)_6(\text{OH})_2$) powder and silica (SiO_2) powder obtained from Fischer Scientific were taken as the precursor materials. The HA and SiO_2 precursor powders had a spherical morphology with an unimodal distribution in the range of 10–30 μm . The pure HA precursor and the thoroughly blended HA- SiO_2 (the ratio of SiO_2 to HA is fixed as 1:3 in weight %) precursor were mixed in a water-based organic solvent (LISI W 15853) obtained from Warren Paint and Color Company (Nashville, TN, USA) and mechanically stirred for 25 min to get a viscous slurry. The slurry was then sprayed onto the polished and clean substrate coupons using an air pressurized spray gun. The sprayed coupons were dried in air to remove the moisture. The thickness of the precursor deposit was maintained at 80 μm for all samples. The precoated samples were finally scanned using a pulsed Nd:YAG laser equipped with a fiber optic beam delivery system to achieve a metallurgical bonding

Table 1 The laser parameters used for the study

Pulse width (ms)	1.0
Average power (W)	80
Spot shape	Rectangular
Spot diameter (μm)	900
Laser scan speed (cm/min)	25; 75; 125
Line spacing (mm)	0.1

between the precursor and the substrate. The pulsed Nd:YAG laser operates in the infrared region with a wavelength of 1064 nm. The processing parameters used for the above process are listed in Table 1. It can be seen from the table that three different laser scan speeds, 25, 75, and 125 cm/min were employed for processing each precursor component.

2.2 Surface characterization

Phase evaluations in the samples were studied using a Philips Norelco X-ray Diffractometer (XRD) with Cu Kα radiation of wavelength 0.15418 nm. The XRD system was operated at 20 kV and 10 mA in a 2θ range of 20–100° using a step size of 0.02° and a count time of 1 s. As laser based processing is often associated with extremely rapid cooling rates (>10³°C/s), the resultant microstructure was expected to produce extremely refined grain structure. Hence, the crystallite size of the coated samples was calculated using the Scherrer formula [27]:

$$t = \frac{0.9\lambda}{B \cdot \cos\theta_B} \tag{1}$$

Here, *t* is the crystallite size of a particular phase, *B* is the broadening of diffraction line measured at half its maximum intensity (radians) at Bragg angle θ_B, and λ is the wavelength of Cu Kα radiation (0.15418 nm). The peaks used for calculating crystallite size were chosen to avoid too much overlapping from different phases. In the above equation, the instrumental broadening is not taken into account as our interest was only to see the effect of laser scan speed on the relative crystallite size.

For micro-structural observation across the cross-section the laser processed samples were sectioned perpendicular to the laser track using a low speed saw. The sectioned samples were then polished with emery papers of different grits ranging from 200 to 1000 μm in succession, followed by disc polishing with colloidal silica of 0.3 and 0.05 μm average particle sizes to get a smoothly polished surface. The polished samples were then etched with 5 vol% HF, 3 vol% HNO₃, and 92 vol% H₂O for 10–20 s by immersion etching to reveal the microstructural features. The micro-structure observations across the cross-section were carried

out using a LEO 1525 scanning electron microscope (SEM) coupled with energy dispersive spectrometer (EDS). The surface roughness of Ti-6Al-4V control and laser processed samples were measured using a Leica Confocal laser microscope. The roughness values are recorded in the form of *R_a* (defined as the arithmetic average of all points of the profile also called the center line average height), and RMS (root-mean-square deviation). Five random scans were done across each sample to get an average and standard deviation within these roughness values.

2.3 Contact angle and surface energy

Contact angle measurements were conducted by a static sessile drop technique using a CAM-Plus^R contact angle goniometer (Chemstruments, Inc. Fairfield, Ohio), equipped with a fiber optic light source and Video camera for imaging. A 3 μl liquid droplet with the diameter of 2 mm was suspended from the tip of the hypodermic syringe on the thoroughly cleaned sample and the advancing contact angle was taken as a measure of wettability. The liquid droplet placed on the sample was allowed to stabilize for 10 s before the reading was taken. The test was conducted at room temperature (26°C) and a minimum of ten contact angle readings were taken from random locations on each sample to minimize the errors in the measurement. Further, the contact angle measurement used in the present case was based on the patented (US patent 5268733) half angle technique which also eliminates the errors associated with the tangential alignment. For surface energy calculations by the contact angle measurement technique, an apolar liquid (diodomethane) and two polar liquids (distilled water and formamide) were used and the calculations were made according to the Van Oss approach [28] using the following equation:

$$\gamma_L(1 + \cos\theta) = 2 \left[(\gamma_S^{LW} \gamma_L^{LW})^{1/2} + (\gamma_S^+ \gamma_L^-) + (\gamma_S^- \gamma_L^+) \right] \tag{2}$$

Here, θ is the contact angle of liquid *L* subtended on solid *S*, γ^{LW} is the apolar component of the surface energy, γ⁺ is the Lewis acid component (electron acceptor), and γ⁻ is the Lewis base component (electron donor). The surface energy components of three standard liquids used in this study are listed in Table 2 [29, 30]. The relationships

Table 2 Surface energy components of the standard liquids used in this study (units mJ/m²)

Liquid	γ _L ^{LW}	γ _L ⁺	γ _L ⁻	γ _L ^{AB}	γ _L
Water	21.8	25.5	25.5	51	72.8
Formamide	39	2.28	39.6	19	58
Diodomethane	51	0	0	0	51

between surface energy γ_s and these components are described below [28]:

$$\gamma_s = \gamma_s^{LW} + \gamma_s^{AB} \quad (3)$$

$$\gamma_s^{AB} = 2\sqrt{\gamma_s^+ \gamma_s^-} \quad (4)$$

The surface energy components of different precursor coated samples were calculated using the above equations.

Finally, in order to correlate the surface energy calculations to the mineralization behavior (bioactivity) of the samples, contact angle between the coated samples and simulated body fluid (SBF) and in vitro bioactivity of the coated samples following immersion in SBF was studied. The SBF solution was prepared by dissolving the reagent grade chemicals in the following order: NaCl (8.026 g), NaHCO₃ (0.352 g), KCl (0.225 g), K₂HPO₄·3H₂O (0.230 g), MgCl₂·6H₂O (0.311 g), CaCl₂ (0.293 g) and Na₂SO₄ (0.072 g) into distilled water (700 ml). The fluid was then buffered to pH = 7.4 at 37°C with tri-hydroxymethylaminomethane (6.063 g) and hydrochloric acid (40 ml). Following SBF immersion, the surfaces of the samples were analyzed using SEM equipped with EDS to study the morphology and elemental composition of the HA precipitates. The EDS analysis was carried out with an electron beam energy of 20 keV.

3 Results and discussions

3.1 Phase evolution

Prior to wettability assays, surface characterization of both 100 wt% HA and 25 wt% SiO₂-HA precursor-coated samples as well as uncoated Ti-6Al-4V control was carried out for several aspects, including phase analysis, surface roughness, microstructure, and surface energy.

Figures 1 and 2 show the X-ray diffraction patterns corresponding to 100 wt% HA and 25 wt% SiO₂-HA precursor samples, respectively, processed with different laser scan speeds of 25, 75, and 125 cm/min. There is no major change in the types of phases with varying laser scan speed for the samples processed with 100 wt% HA as precursor material (Fig. 1). Apart from the retention of original precursor (HA phase), the various other phases evolved are CaTiO₃, Ca₃(PO₄)₂, TiO₂ (Anatase), TiO₂ (Rutile), Al₂O₃, and CaO. Although there is no change in phase constituents, the peak intensities varied with varying laser scan speed. Unlike the XRD results of 100 wt% HA sample (Fig. 1), the phase constituents of 25 wt% SiO₂-HA samples (Fig. 2) show dependence on the laser scan speed. For the samples processed with higher laser speed of 75 and 125 cm/min, although the peak intensities varied no major change in the types of phases evolved. The main

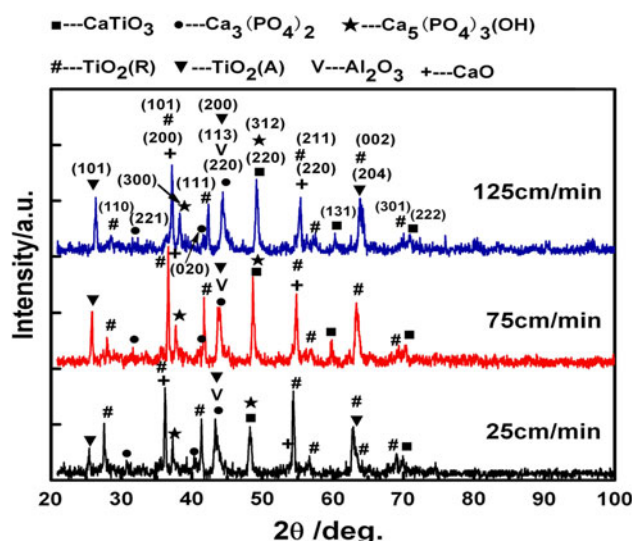


Fig. 1 XRD pattern of 100 wt% HA precursor after processed with different laser scan speed

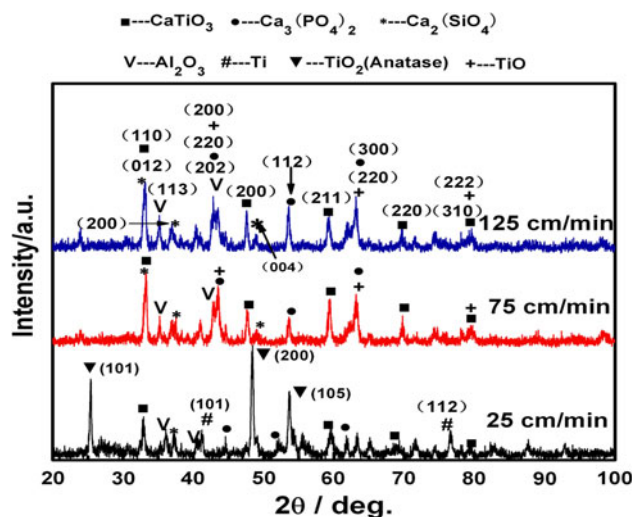
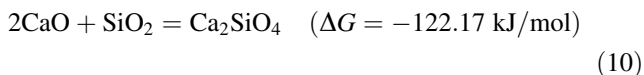
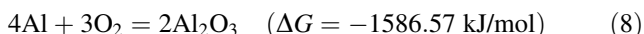
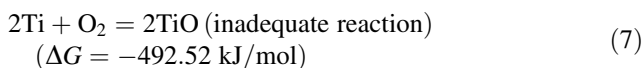
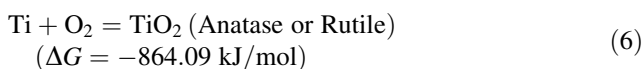
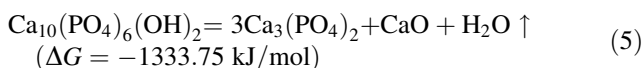


Fig. 2 XRD pattern of 25 wt% SiO₂-HA precursor after processed with different laser scan speed

phases are identified as CaTiO₃, Ca₃(PO₄)₂, Ca₂SiO₄, Al₂O₃, and TiO. On the contrary, for the samples processed with slower speed of 25 cm/min, the major phase presented in the coating is TiO₂ (Anatase), and the peak intensities corresponding to such phases as CaTiO₃, Ca₃(PO₄)₂, and Ca₂SiO₄ are relatively weak. Thus, it appeared that at higher range of laser scan speed (75–125 cm/min), the phase constituent is minimally affected by the speed for both 100 wt% HA and 25 wt% SiO₂-HA precursor samples. Whereas at slower laser scan speed (<25 cm/min) the laser beam residence time on the sample surface being longer, the surface temperature rises to the level possibly leading to substantial amount of coating precursor material

evaporation followed by oxidation of the substrate material for formation of more amount of TiO₂. Also, as the laser processing is carried out in an ambient atmosphere under higher energy laser beam, a small portion of the substrate material (Ti-6Al-4V) always gets melted and oxidized to form Al₂O₃ for both the precursor material compositions.

The effect of addition of SiO₂ in HA precursor is further realized through the absence of HA and CaO in laser processed 25 wt% SiO₂-HA samples (Fig. 2) compared to laser processed 100 wt% HA samples (Fig. 1). This phenomenon can be explained on the basis of the following possible primary and intermediate reactions between the material systems employed in the present work.



From the above equations, it is clear that the retention of HA precursor phase depends on the Eqs. 5, 6, 9, and 10. The more HA takes part in Eq. 5, the less it will be retained in the coating. From Eqs. 9 and 10 it is clear that for 100 wt% HA samples, only TiO₂ react with CaO, where as in 25 wt% SiO₂-HA samples SiO₂ addition will consume more CaO resolved from HA. This is likely to accelerate the resolving process of HA, and the reaction process between CaO and SiO₂, leading to less or no retention of HA or SiO₂ in the coating. The above intermediate reactions (Eqs. 9, 10) during laser processing of 25 wt% SiO₂-HA precursor, therefore, results in generation of Ca₂SiO₄ in the coating (Fig. 2).

The average crystallite size of 100 wt% HA and 25 wt% SiO₂-HA samples was calculated using the Scherrer formula as stated in Eq. 1. The results are presented in Fig. 3. It is obvious that the crystallite size in 25 wt% SiO₂-HA samples is significantly smaller (~28%) than that of 100 wt% HA samples, which indicates the effect of SiO₂ addition on grain refinement. SiO₂ has long been added to BaTiO₃ to reduce the grain size [31]. In the work by M.A.Zubair et al. [32], it was reported that SiO₂ addition can develop the grain boundaries and reduce the grain size. Kaishu Guan et al. [33] have studied the enhanced effect and mechanism of SiO₂ addition in super-hydrophilic property of TiO₂ film. The authors reported that the grain

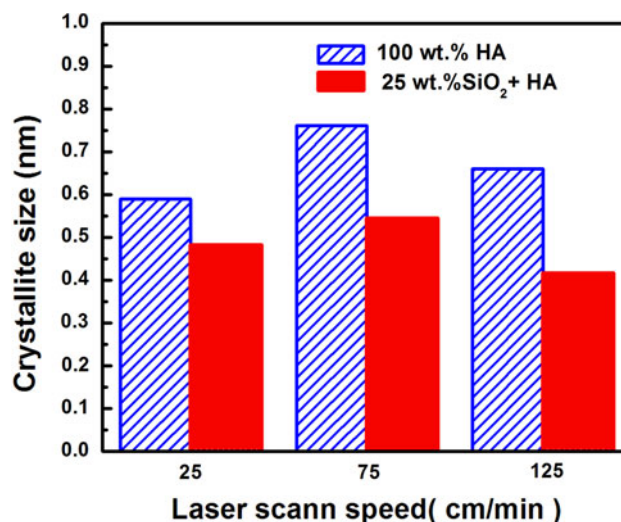


Fig. 3 Crystallite size of different samples processed with different laser scan speed

growth of TiO₂ crystal is suppressed by the addition of SiO₂ which in turn led the particle size of TiO₂ to become smaller and thereby its improved hydrophilic behavior. In the work by Takeli et al. [34, 35], it was reported that grain-growth rate could be controlled by the addition of SiO₂ and the grain size decreased with increasing SiO₂. The grain growth kinetics of both 100 wt% HA samples and 25 wt% SiO₂-HA samples can be semi quantitatively described by the grain growth model as described below [36]:

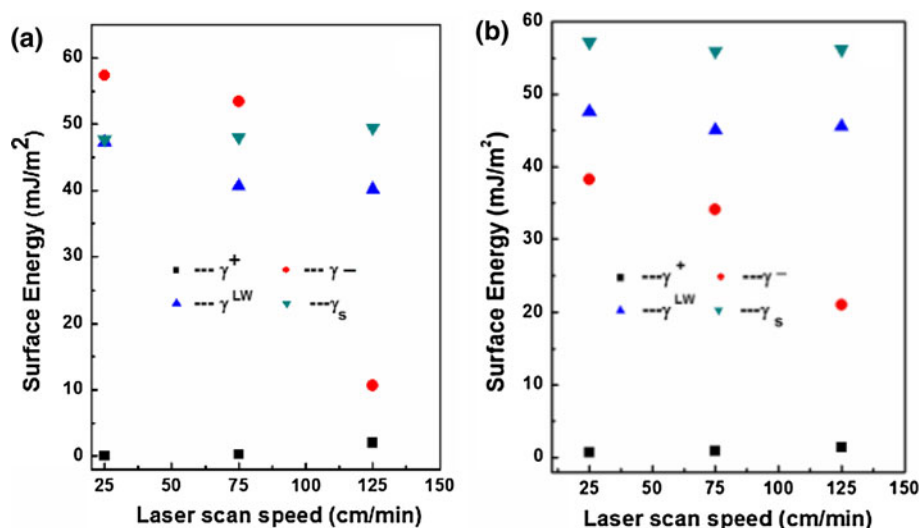
$$G^n - G_0^n = kt \quad (11)$$

Here G is the average grain size, G_0 is the initial grain size, k is a rate constant, n is a constant for a given grain-growth mechanism, and t is the crystallization time. From Eq. 11 it is clear that for a given initial grain of size G_0 the average grain size G depends on the crystallization time t . A lower crystallization time t corresponds to a smaller average grain size G . It was reported that the addition of SiO₂ can accelerate the material transfer and results in a fast microstructural evolution [37], and also control microstructure by suppressing abnormal grain growth [38]. Hence, it is clear from the above results that SiO₂ addition can reduce the crystallization time, which in turn attributes to a smaller crystallite size. In the present work, laser-based processing is inherently associated with the rapid cooling rates [39], thus further expected to contribute substantially reduced crystallization time and crystallite size.

3.2 Surface energy and surface roughness

The variation of surface energy components (γ^+ , γ^- , γ^{LW} , and γ_s) as a function of laser scan speed for the 100 wt% HA and 25 wt% SiO₂-HA samples are illustrated in Fig. 4.

Fig. 4 Surface energy components for **a** 100 wt% HA and **b** 25 wt% SiO₂-HA coatings



For 100 wt% HA samples, the dispersive component (γ^{LW}) decreases with increasing laser scan speed and remains in the range of 40–47 mJ m⁻². The basic polar component (γ^-) also follows a decreasing trend with increasing laser scan speed from 25 to 125 cm/min. The acidic polar component (γ^+) has values less than 2.0 mJ m⁻² and follows a slightly increasing trend with increasing laser scan speed. The surface free energy of the 100 wt% HA samples is around 48 mJ m⁻² (Table 3). For 25 wt% SiO₂-HA samples, the dispersive component floats between 45 and 47 mJ m⁻². The basic polar component follows the same trend as with the 100 wt% HA samples. Compared to 100 wt% HA samples, 25 wt% SiO₂-HA samples present lower acidic polar component (its acidic polar component is less than 1.4 mJ m⁻²) and higher surface free energy (around 56 mJ m⁻²). It can be seen from Table 3 that for both 25 wt% SiO₂-HA and 100 wt% HA precursor, the surface free energy varied slightly at different laser scan speeds. This can be attributed to the minor variation in phase constituents with the varying laser scan speed. As described earlier from the XRD studies (Fig. 2), the addition of SiO₂ in the precursor leads to the formation of dicalcium silicate (Ca₂SiO₄) in the matrix of various other phases. The formation of such a wetting silicate based phase at the grain boundaries owing to the addition of SiO₂ has already been reported [32]. This further might have contributed to the increase in surface free energy for 25 wt% SiO₂-HA samples as compared to 100 wt% HA samples (Table 3). Another possible reason for the variation in surface energy for these samples may also be due to the grain size. As described above (Fig. 3), the average grain size of 25 wt% SiO₂-HA samples is smaller than that of the 100 wt% HA samples. Therefore, more grain boundary grooves were formed with SiO₂ addition leading to formation of more pinning of tripple lines. These pinned tripple lines act as

open capillaries to reinforce wetting [40]. The work by Ishida [41] also stated that grain size strongly influences the grain boundary segregation. In the work by Tekeli et al. [34], it was also stated that SiO₂ addition results in a lower grain boundary cohesive strength and a higher grain boundary mobility and energy. Hence, 25 wt% SiO₂-HA possessed a higher surface energy value (55.94–57.21 mJ/m²) compared to 100 wt% HA samples (47.71–49.47 mJ/m²) and the Ti-6Al-4V control (34.19 mJ/m²). Also, as described earlier from the XRD results (Figs. 1, 2), it can be realized that following laser processing the coating is not phase pure and is composed of various phases. Hence, each of these phases is expected to contribute to the wetting behavior and thereby its surface energy. However, in the present work following laser processing of both the precursor materials, most of the phases such as CaTiO₃, Ca₃(PO₄)₂, and TiO₂ except Ca₂SiO₄ are found common. Hence, the improved wetting behavior for the 25 wt% SiO₂-HA precursor as compared to 100 wt% HA can only be attributed to the presence of Ca₂SiO₄ following laser processing.

The surface microstructure and the cross-sectional microstructure of 100 wt% HA and 25 wt% SiO₂-HA samples processed at laser scan speed of 125 cm/min are presented in Fig. 5. The surface roughness values, R_a , and RMS are listed in Table 3. It can be seen that the surface roughness values of both 100 wt% HA samples and 25 wt% SiO₂-HA samples are larger than that of the Ti-6Al-4V control. In addition, from the SEM cross-sectional views (Fig. 5c, d), less number of cracks were observed in 25 wt% SiO₂-HA sample compared to 100 wt% HA sample. It indicates that SiO₂ addition can not only refine the grain size, but also can suppress the cracks formation. This is in compliance with the work by Izquierdo-Barba [42], where the authors reported that more amount of Si in the coating

Table 3 Surface roughness, contact angle with SBF, and surface energy of the samples

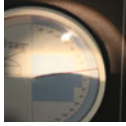
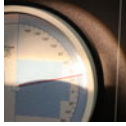
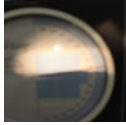
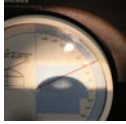
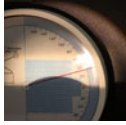
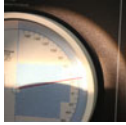
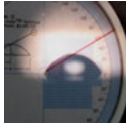
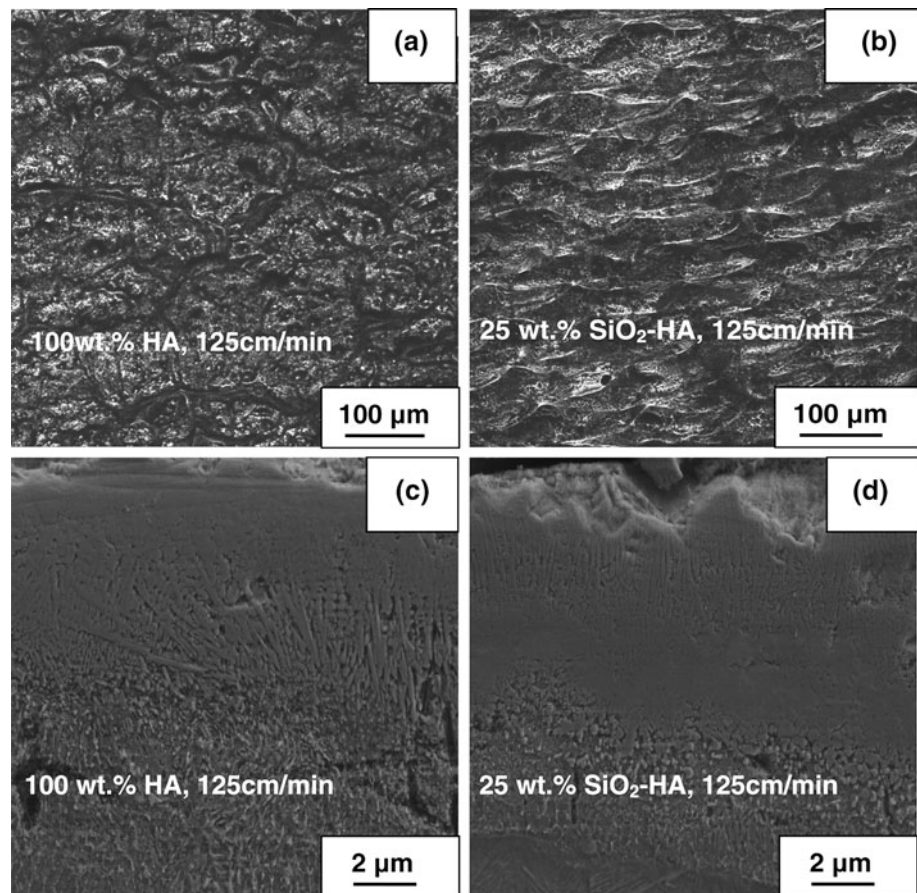
Precursor	Laser speed (cm/min)	R_a (μm)	RMS (μm)	Contact angle in different fluid				Surface energy (mJ/m^2)
				Distilled water	Formamide	Dioiodomethane	Simulate body fluid (SBF)	
25 wt% SiO_2 -HA	125	2.0 ± 1.1	12.4 ± 4.0	48.5 ± 0.6	18.5 ± 0.6	26.9 ± 0.8	21.2 ± 1.4	56.20 ± 0.97
								
	75	1.8 ± 0.8	12.1 ± 3.2	36.6 ± 0.4	17.2 ± 0.8	28.3 ± 1.0	26.4 ± 1.3	55.94 ± 0.87
								
	25	3.7 ± 1.8	18.0 ± 3.5	35.0 ± 0.7	14.6 ± 0.9	21.2 ± 0.5	19.2 ± 1.8	57.21 ± 0.74
								
100 wt% HA	125	1.4 ± 0.2	11.6 ± 1.0	62.4 ± 0.5	32.4 ± 0.7	39.2 ± 1.3	40.8 ± 1.0	49.47 ± 0.18
								
	75	4.1 ± 0.7	16.8 ± 1.2	26.8 ± 1.8	30.6 ± 1.2	38.2 ± 0.6	32.8 ± 1.9	48.01 ± 0.92
								
	25	3.3 ± 1.9	13.6 ± 1.0	20.6 ± 0.9	28.3 ± 0.5	22.3 ± 0.8	31.0 ± 1.8	47.71 ± 0.21
								
Ti-6Al-4V control		0.3 ± 0.07	9.47 ± 0.2	82.6 ± 0.1	57.4 ± 0.1	53 ± 0.04	$55.7 \pm \pm 1.6$	34.19 ± 0.05
								

Fig. 5 Surface texture images and SEM micrographs of 100 wt% HA samples and 25 wt% SiO₂-HA samples processed with laser scan speed of 125 cm/min



can reduce the porosity of the surface leading to reduced presence of cracks across the cross-section.

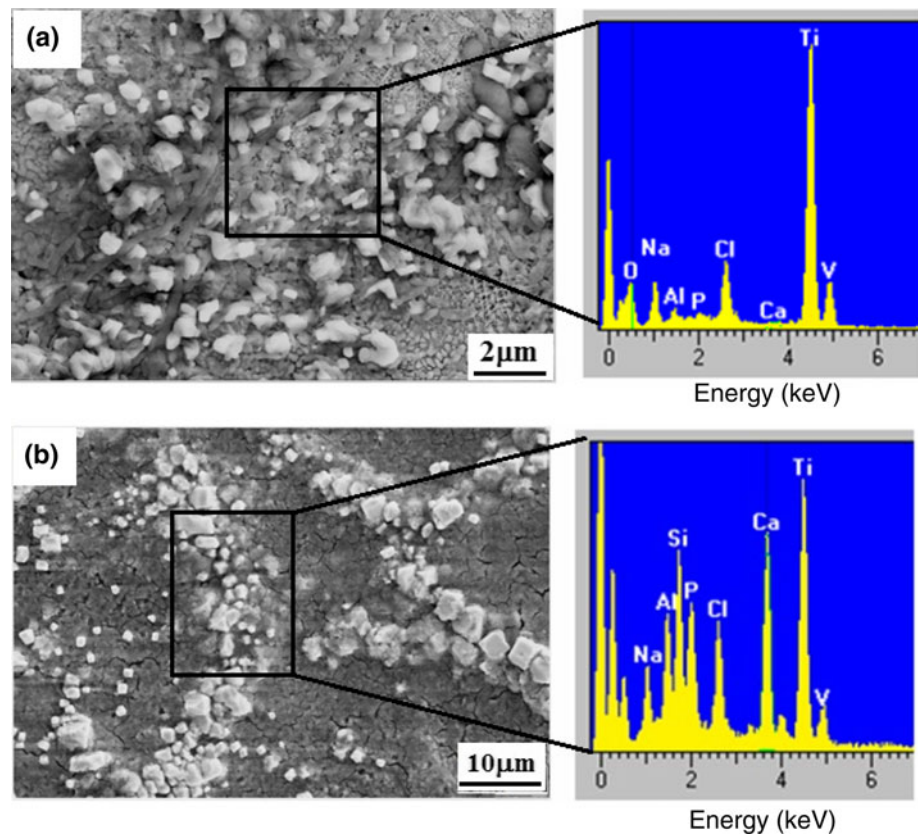
3.3 Wettability and in vitro bioactivity

When a biomaterial is implanted into a biological system, among the plethora of events that takes place, the first and the foremost one is the wetting of the implant material by the physiological fluids. This further determines the degree and confirmation of specific proteins which in turn influence recruitment and activation of cells and stimulation of new tissue development [43, 44]. Hence, besides analyzing the phase constituents, surface roughness, and surface free energies, understanding the wettability of the coatings with SBF were also the important aspects of this work. Further, the contact angle measurements obtained from SBF liquid can also provide an understanding of the effect of SiO₂ addition on the wetting behavior. Table 3 represents the contact angle measurements and corresponding light optical images of the liquid droplet shadow on 100 wt% HA samples, 25 wt% SiO₂-HA samples, and the control (untreated Ti-6Al-4V). The results (Table 3) demonstrated

improved wettability for the laser processed samples (100 wt% HA and 25 wt% SiO₂-HA samples) as compared to the control (untreated Ti-6Al-4V). Furthermore, compared to 100 wt% HA samples, 25 wt% SiO₂-HA samples indicated a more hydrophilic behavior (better improved wettability). As discussed earlier, the addition of SiO₂ not only influenced the phase constituents and the surface roughness, but also contributed to increase in the surface energy. This increase in surface free energy of 25 wt% SiO₂-HA samples was responsible for improved wettability of the coatings in SBF.

The wettability of the coatings was finally correlated to its mineralization or in vitro bioactivity by immersing the samples in SBF and analyzing for the precipitation of an apatite like phase. The mineralized layer or the precipitates on the 100 wt% HA sample and 25 wt% SiO₂-HA sample after 7 day immersion in SBF is shown in Fig. 6. The presence of a cuboidal like apatite crystallites can be clearly seen on the surfaces of 100 wt% HA and 25 wt% SiO₂-HA samples (Fig. 6a, b, respectively). The EDS spectra from a selected region indicates the presence of various elemental species such as Ca, P, Na, Cl, Al, O, Ti and V in the precipitated layer. In the current work,

Fig. 6 SEM morphological analysis and corresponding EDS results on **a** 100 wt% HA sample and **b** 25 wt% SiO₂-HA sample after 7 days immersion in SBF



as the EDS analysis are carried out using an electron beam energy of 20 keV, a significant amount of material underneath the coating is sputtered resulting in detection of the sub-surface elemental species such as Ti and V in the spectrum. The EDS spectra from the mineralized surface of 100 wt% HA demonstrated for a small amount of Ca and P with a Ca/P atomic ratio of 0.62. In contrast, the selected region EDS spectra of the mineralized layer on 25 wt% SiO₂-HA demonstrated strong presence of Ca and P with a Ca/P atomic ratio of 1.68. As, the Ca/P atomic ratio of the mineralized layer on 25 wt% SiO₂-HA is close to that of the Ca/P atomic ratio of stoichiometric HA (1.67), it was therefore confirmed that the cuboid like precipitates were an apatite like phase and hence the sample is more bioactive as compared to the 100 wt% HA sample. Thus, the effects of SiO₂ addition on the phase constituents, grain size, and surface free energy can be systematically correlated to their consequential effects on wettability and in vitro bioactivity of HA coated Ti-6Al-4V alloy samples. Further analysis for mineralization kinetics and in vitro biocompatibility of the laser processed samples are being studied by exposing the samples to SBF for different time periods and culturing of mouse MC3T3-E1 pre-osteoblast cells, respectively. The results pertaining to the above efforts are being

simultaneously prepared in a separate paper for publication in a referred journal.

4 Conclusions

The process of laser direct melting of Ca-P and SiO₂/Ca-P precursors on Ti-6Al-4V substrate resulted in the formation of various phases, such as CaTiO₃, Ca₃(PO₄)₂, TiO₂ (Rutile and Anatase), Al₂O₃, and Ca₂SiO₄ within the coatings. With SiO₂ addition in the precursor, a new phase (Ca₂SiO₄) was formed. No significant variation of the phase type with the laser speed variation was observed. Addition of SiO₂ in the precursor also produced more grain boundary grooves, resulting in a rough surface (higher RMS value) compared to the titanium control. Furthermore, the presence of SiO₂ in the precursor led to formation of the smaller average crystallite size and reduced cracking in the coating. The samples coated with SiO₂-HA precursor demonstrated a higher surface free energy and hence better wettability compared to the samples coated with pure HA precursor and the Ti-6Al-4V control. Additionally, the improved wettability and in vitro bioactivity of the samples with SiO₂ addition is also clearly due to the formation of Ca₂SiO₄ at the grain boundaries, the finer grain size and the higher surface roughness.

Acknowledgments A support to Yuling Yang during this work at the University of Tennessee by National Science Foundation of China for Young Scholars (Grant # 50801012) is highly acknowledged. Yuling Yang also thanks China Scholarship Council (CSC) and Northeastern University (NEU) for providing a financial support as visiting scholar at the University of Tennessee.

References

1. Driessens FCM, Verbeeck RMH. *Biomaterials*. Boca Raton: CRC Press; 1990. p. 5.
2. Foppiano S, Marshall SJ, Marshall GW, Saiz E, Tomsia AP. The influence of novel bioactive glasses on in vitro osteoblast behavior. *J Biomed Mater Res*. 2004;71:242–9.
3. Bosetti M, Cannas M. The effect of bioactive glasses on bone marrow stromal cells differentiation. *Biomaterials*. 2005;26:3873–9.
4. Hattar S, Asselin A, Greenspan D, Oboeuf M, Berdal A, Sautier JM. Potential of biomimetic surfaces to promote in vitro osteoblast-like cell differentiation. *Biomaterials*. 2005;26:839–48.
5. Lopez-Heredia MA, Legeay G, Gaillard C, Layrolle P. Radio frequency plasma treatments on titanium for enhancement of bioactivity. *Acta Biomater*. 2008;4:1953–62.
6. Pecheva Emilia V, Pramatarova Liliana D, Maitz Manfred F, Pham Mihn T, Kondyurin Aleye V. Kinetics of hydroxyapatite deposition on solid substrates modified by sequential implantation of Ca and P ions: Part I. FTIR and Raman spectroscopy study. *Appl Surf Sci*. 2004;235:176–81.
7. Weng J, Liu Q, Wolke JGC, Zhang XD, de Groot K. Formation and characteristics of the apatite layer on plasma-sprayed hydroxyapatite coatings in simulated body fluid. *Biomaterials*. 1997;18:1027–35.
8. Bang HG, Kim SJ, Park SY. Biocompatibility and the physical properties of bio-glass ceramics in the $\text{Na}_2\text{O-CaO-SiO}_2\text{-P}_2\text{O}_5$ system with CaF_2 and MgF_2 additives. *J Ceram Process Res*. 2008;9:588–90.
9. Hristov JH, Bogdanov BI, Chomakov IG, Markov IG, Markovska IG. Drawing standard curve for quantitative determination of the crystalline phase in wollastonite glass ceramics. *J Balkan Tribology Assoc*. 2009;15:347–54.
10. Choi SW, Hong SH, Kim YJ. Characterization of $\text{Ca}_2\text{SiO}_4\text{:Eu}^{2+}$ phosphors synthesized by polymeric precursor process. *J Am Ceram Soc*. 2009;92:2025–8.
11. Carlise E. Si: an essential element for the chick. *Science*. 1972;178:619–21.
12. Schwarz K, Milne D. Growth promoting effects of Si in rats. *Nature*. 1972;239:333–4.
13. Seaborn C, Nielson F. Si deprivation decreases collagen formation in wounds, bone and ornithine transaminase enzyme activity in liver. *Biol Trace Elem Res*. 2002;89:251–61.
14. Schwarz K. A bound form of Si in glycosaminoglycans and polyuronides. *Proc Nat Acad Sci USA*. 1973;70:1608–12.
15. Pietak AM, Reid JW, Stott MJ, Sayer M. Silicon substitution in the calcium phosphate bioceramics. *Biomaterials*. 2007;28:4023–32.
16. Tanizawa Y, Suzuki T. Effects of silicate ions on the formation and transformation of calcium phosphates in neutral aqueous solutions. *J Chem Soc Faraday Trans*. 1995;91:3499–503.
17. Damen J, Ten Cate J. Silica-induced precipitation of calcium phosphate in the presence of inhibitors of hydroxyapatite formation. *J Dent Res*. 1992;71:453–7.
18. Sayer M, Stratilatov A, Reid J, Calderin L, Stott M, Yin X, et al. Structure and composition of silicon stabilized tricalcium phosphate. *Biomaterials*. 2002;24:369–82.
19. Gibson I, Best S, Bonfield W. Effect of silicon substitution on the sintering and microstructure of hydroxyapatite. *J Am Ceram Soc*. 2002;85:2771–7.
20. Tang X, Xiao X, Liu R. Structural characterization of silicon substituted hydroxyapatite synthesized by hydrothermal method. *Mater Lett*. 2005;59:3841–6.
21. Reid J, Tuck L, Sayer M, Fargo K, Hendry J. Synthesis and characterization of single-phase silicon-substituted alpha-tricalcium phosphate. *Biomaterials*. 2006;27:2915–6.
22. Cheng XM, Nie BM, Kumar S. Preparation and bioactivity of SiO_2 functional films on titanium by PACVD. *Trans Nonferrous Met Soc China*. 2008;18:627–30.
23. Acros D, Rodriguez-Carvajal J, Vallet-Regi M. Silicon incorporation in hydroxyapatite obtained by controlled crystallization. *Chem Mater*. 2004;16:2300–8.
24. Pietak A, Sayer M. Crystallization kinetics of Si-TCP bioceramic. *J Mater Sci*. 2004;39:2443–9.
25. Patel N, Best S, Bonfield W, Gibson I, Hing K, Damien E, et al. A comparative study on the in vivo behavior of hydroxyapatite and silicon substituted hydroxyapatite granules. *J Mater Sci Mater Med*. 2002;13:1199–206.
26. Thian ES, Ahmad Z, Huang J, Edirisinghe MJ, Jayasinghe SN, Ireland DC, Brooks RA, Rushton N, Bonfield W, Best SM. The role of surface wettability and surface charge of electrosprayed nanoapatites on the behavior of osteoblasts. *Acta Biomater*. 2010;6:750–5.
27. Cullity BD. *Elements of X-ray diffraction*. 2nd ed. Reading: Addison-Wesley Publishing Company, Inc; 1978. p. 284.
28. Van Oss CJ, Good RJ, Chaudhury MK. Additive and non additive surface tension components and the interpretation of contact angles. *Langmuir*. 1988;4:884–91.
29. Randeniya LK, Bendavid A, Martin PJ, Amin MS, Preston EW, Ismail FSM, Coe S. Incorporation of Si and SiO_x into diamond-like carbon films: impact on surface properties and osteoblast adhesion. *Acta Biomater*. 2009;5:1791–7.
30. Van Oss CJ, Giese RF Jr, Good RJ. Reevaluation of the surface tension components and parameters of polyacetylene from contact angle of liquids. *Langmuir*. 1990;6:1711–3.
31. Roseman RD, Mukherjee N. PTCR effect in BaTiO_3 : structural aspects and grain boundary potentials. *J Electroceram*. 2003;10:117–35.
32. Zubair MA, Leach C. The effect of SiO_2 addition on the development of low- Σ grain boundaries in PTC thermistors. *J Eur Ceram Soc* (in press, available on line).
33. Guan K, Lu B, Yin Y. Enhanced effect and mechanism of SiO_2 addition in super-hydrophilic property of TiO_2 films. *Surf Coat Technol*. 2003;173:219–23.
34. Tekeli S, Erdogan M, Aktas B. Structural evolution in 8 mol% Y_2O_3 -stabilized cubic zirconia (8YSCZ) with SiO_2 addition. *Mater Sci Eng A*. 2004;386:1–9.
35. Tekeli S, Boyacıoğlu T, Güral A. The effect of silica doping on the microstructure and mechanical properties of c- $\text{ZrO}_2/\text{SiO}_2$ composites. *Ceram Int*. 2008;34:1959–64.
36. Brook RJ. *Treatise on materials science and technology*. New York: Academic Press; 1976.
37. Yoo Y-S, Kim H, Kim D-Y. Effect of SiO_2 and TiO_2 addition on the exaggerated grain growth of BaTiO_3 . *J Eur Ceram Soc*. 1997;17:805–11.
38. Hussaina S, Anis-ur-Rehman M, Maqsooda A, Awan MS. The effect of SiO_2 addition on structural, magnetic and electrical properties of strontium hexa-ferrites. *J Cryst Growth*. 2006;297:403–10.
39. Paital SR, Dahotre NB. A thermal model for laser interaction with thick dielectric film on metallic substrate: application to Ca-P layer on Ti alloy. *J Alloys Compd*. 2009;487:499–503.

40. Eustathopoulos N, Nicholas MG, Drevet B. Wettability at high temperatures. 2nd ed. New York: Pergamon; 1999. p. 108.
41. Ishida K. Effect of grain size on grain boundary segregation. *J Alloys Compd.* 1996;235:244–9.
42. Izquierdo-Barba I, Conde F, Olmo N, Lizarbe MA. Vitreous SiO₂-CaO coatings on Ti6Al4V alloys: reactivity in simulated body fluid versus osteoblast cell culture. *Acta Biomater.* 2006;2: 445–55.
43. Ducheyne P, Qui Q. Bioactive ceramics: the effect of surface reactivity on bone formation and function. *Biomaterials.* 1999;20: 2287–303.
44. Hench L. Surface reaction kinetics and adsorption of biological moieties: a mechanistic approach to tissue attachment. In: Davies JE, editor. *The bone biomaterial interface.* Toronto: University of Toronto Press; 1991. p. 33–42.